chemosensors

MDPI

Article

Ni–Co–Te Nanocomposites with Multi-Dimensional Hierarchical Structure for Electrochemical Acetaminophen Sensing

Jin-Jia Ye [1], Zhi-Yuan Wang [1], Han-Wei Chang [2,3,*] and Yu-Chen Tsai [1,*]

[1] Department of Chemical Engineering, National Chung Hsing University, Taichung 40227, Taiwan
[2] Department of Chemical Engineering, National United University, Miaoli 360302, Taiwan
[3] Pesticide Analysis Center, National United University, Miaoli 360302, Taiwan
* Correspondence: hwchang@nuu.edu.tw (H.-W.C.); yctsai@dragon.nchu.edu.tw (Y.-C.T.); Tel.: +886-37-382216 (H.-W.C.); +886-4-22857257 (Y.-C.T.)

Abstract: In this study, Ni–Co–Te nanocomposites with multi-dimensional hierarchical structure were successfully prepared using a hydrothermal method. Ni–Co–Te nanocomposites used as electrode materials afford enhanced electroactive properties for electrochemical acetaminophen sensing. Field emission scanning electron microscopy (FESEM), field emission transmission electron microscopy (FETEM), X-ray photoelectron spectroscopy (XPS), and X-ray diffraction (XRD) were used to characterize the morphological and structural properties to boost their further promotion in acetaminophen sensing. The electrochemical performance of Ni–Co–Te nanocomposites was characterized by electrochemical measurements (cyclic voltammetry (CV) and differential pulse voltammetry (DPV)). The lower electronegativity of the telluride atom and unique structural features of Ni–Co–Te nanocomposites endow the materials with promising performance in acetaminophen sensing (including linear range from 2.5 to 1000 μM, sensitivity of 0.5 $\mu A \mu M^{-1} cm^{-2}$, limit of detection of 0.92 μM, and excellent selectivity). The results indicated that Ni–Co–Te nanocomposites can serve as promising electrode materials for practical application in electrochemical acetaminophen sensing.

Keywords: Ni–Co–Te nanocomposites; electrochemical acetaminophen sensing; electronegativity; structural features

Citation: Ye, J.-J.; Wang, Z.-Y.; Chang, H.-W.; Tsai, Y.-C. Ni–Co–Te Nanocomposites with Multi-Dimensional Hierarchical Structure for Electrochemical Acetaminophen Sensing. *Chemosensors* **2022**, *10*, 336. https://doi.org/10.3390/chemosensors10080336

Academic Editor: Constantin Apetrei

Received: 26 July 2022
Accepted: 15 August 2022
Published: 17 August 2022

1. Introduction

Acetaminophen (N-acetyl-p-aminophenol, paracetamol) is the most frequently used over-the-counter (OTC) analgesic and antipyretic medication in the short-term and moderately effective treatment of fever and pain management for patients. The analgesic effect of acetaminophen is believed to act through a cyclooxygenase (COX) inhibitor in the central nervous system (CNS) involved in the transport of endocannabinoid and vanilloid, promoting its use as a mild sedative and/or general anesthetic [1,2]. However, mounting evidence (albeit controversial) supports that overdosing of acetaminophen (a dosage of 3~4 g daily is recommended for an adult) leads to the accumulation of toxic intermediary metabolites linked with increased risk of various dangerous side effects including asthmatic symptoms [3] and acute liver/kidney damage [4]. In Taiwan, more than approximately 400 million doses of annual prescriptions for acetaminophen-containing products were dispensed from 2016 to 2020 to treat acute and chronic pain. According to recent reports [5–9], the global yearly acetaminophen market, involving a broad range of market value estimations, was estimated to be approximately USD 100~800 million. For these reasons, acetaminophen was listed by the World Health Organization (WHO) as an essential medicines [9]. This supports the best evidence that there is a current over-reliance on acetaminophen for humans to relieve pain. Therefore, there is an urgent need for the development of accurate and rapid analytical methods to determine acetaminophen levels

in various pharmaceutical sample analyses and human serum. In recent years, various analytical methods have commonly been used to determine acetaminophen, including high-performance liquid chromatography [10], near-infrared spectrometry [11], ultraviolet–visible (UV–vis) spectrometry [12], and gas chromatography-mass spectrometry [13]. These analytical methods exhibit excellent sensitivity, selectivity, and reliable results for acetaminophen detection. Previous studies have also indicated that use of an electrochemical method may be a choice procedure for performing acetaminophen sensing due to its low cost, easy fabrication, excellent sensitivity/selectivity, good reproducibility, and excellent accuracy/portability of equipment [14–17]. Therefore, integration of these analytical methods (including the electrochemical method) could open new possibilities in acetaminophen sensing for rapid screening and confirmatory testing in practical application. According to previous reports, the development of electrochemical acetaminophen sensing largely depends on the optimal match of promising electrode materials, including noble metals [18,19], carbon materials [20,21], and transition metal compounds [22,23]. Considering sustainable development issues, novel well-defined electrode materials based on earth-abundant transition metal compounds, owing to their higher exposed electrocatalytic active sites, have been considered as ideal electrode materials and strong contenders for integration into electrochemical sensing [24–26]. Among transition metal compounds, transition metal tellurides possess a high degree of covalency in the metal–telluride bond due to the lower electronegativity of telluride (2.1) compared with Se (2.55), S (2.58), and O (3.44), meaning there is a higher energy and weaker attraction of electrons in the 3d orbitals of transition metal atoms in transition metal tellurides, than transition metal compounds containing oxides, sulfides, and selenides. Thus, lower energies are required to charge electrons occurring within electrochemical reactions, which promotes stronger reaction kinetics between the covalency of metal−ligand bonding, with a greatly improved electrochemical performance [27,28]. Such unique characteristics render transition metal tellurides accessible for promising application in the field of electrochemistry, including water splitting [29], CO_2 reduction [30], and rechargeable batteries [31]. To date, only a few reports can be found regarding transition metal tellurides and their predominantly electrochemical application, which greatly motivates us to explore their application in the field of electrochemical sensing.

In this work, Ni–Co–Te nanocomposites were successfully prepared by hydrothermal method. Further, Nafion was employed as a coating material to obtain well-dispersed Ni–Co–Te nanocomposites firmly attached to the working electrode surface. The as-prepared materials were used as electrochemically active materials to detect acetaminophen via electrochemical methods. Te atoms in the Ni–Co–Te nanocomposites with relatively lower electronegativity may reflect a higher degree of metal−ligand bonding, to further improve the electrochemical performance. It is expected that Ni–Co–Te nanocomposites could be a promising electrode material for electrochemical acetaminophen sensing.

2. Materials and Methods

2.1. Reagents

Cobalt (II) chloride hexahydrate ($CoCl_2 \cdot 6H_2O$) and nickel chloride hexahydrate ($NiCl_2 \cdot 6H_2O$) were obtained from Alfa Aesar (Ward Hill, MA, USA). Tellurium powder, Nafion solution (5 wt % in mixture of lower aliphatic alcohols and water), ethylenediamine, hydrazine, acetaminophen (AC), D-(+)-Glucose (Glu), dopamine hydrochloride (DA), uric acid (UA), and L-ascorbic acid (AA) were purchased from Sigma-Aldrich (St. Louis, MO, USA). Anhydrous ethanol (C_2H_5OH, 99.5%) was purchased from J.T. Baker (Phillipsburg, NJ, USA). The deionized water (DI water) was produced from a Milli-Q water purification system (Millipore, MA, USA). All chemicals were analytical grade and were used as received without further purification.

2.2. Preparation of Ni–Co–Te Nanocomposites

Ni–Co–Te nanocomposites were successfully synthesized by using Ni–Co precursors through a hydrothermal process. First, 0.411 g $NiCl_2 \cdot 6H_2O$ and 0.409 g $CoCl_2 \cdot 6H_2O$ were dissolved in 30 mL DI water under ultrasonic treatment for 30 min to form a homogenous solution. Second, 0.235 g tellurium powder was dispersed to 8 mL ethylenediamine. Then, the mixture was gradually added into Ni–Co precursors under ultrasonic treatment for 30 min. Hydrazine, as reducing reagent, was slowly added to the above solution with continuous stirring, which caused the formation of black-colored precipitation. Then, the obtained mixture was transferred into a 100 mL Teflon-lined stainless steel autoclave and heated at 180 °C for 24 h. The resulting Ni–Co–Te nanocomposites were separated by centrifugation, washed with ethanol and DI water (three times), dried in an oven at 60 °C, and collected for subsequent treatment.

2.3. Preparation of Modified Electrode

The preparation procedure of as-prepared samples modified GCE was as follows: first, bare GCE was carefully polished with alumina powders (0.3 and 0.05 μm) on a polishing cloth, then was rinsed thoroughly with distilled water, sonicated in ethanol and distilled water (three times), and dried at ambient temperature. The resulting Ni–Co–Te nanocomposites were dispersed into a 0.5 wt % Nafion solution by ultrasonication to form the stabilized and well-dispersed Ni–Co–Te/Nafion solution. Then, the mixture solution (10 μL) was dropped on the surface of bare GCE and air dried at ambient temperature. Finally, a Ni–Co–Te/Nafion-modified GCE was obtained for the following electrochemical measurements.

2.4. Apparatus

The morphology was characterized using field emission scanning electron microscopy (FESEM, JSM-7410F, JEOL, Akishima, Japan) and field emission transmission electron microscopy (FETEM, JEM-2100F, JEOL, Akishima, Japan). The chemical structure and composition were determined by X-ray photoelectron spectroscopy (XPS, PHI-5000 Versaprobe, ULVAC-PHI, Chigasaki, Japan). X-ray diffraction (XRD) patterns were recorded using a D8 Discover (Bruker) X-ray diffractometer with Cu Kα radiation. Electrochemical measurements were performed using a three-electrode system comprised of as-prepared samples of modified glassy-carbon electrode (GCE, 3.0 mm in diameter, Tokai Carbon, Tokyo, Japan), a platinum wire counter electrode, and an Ag/AgCl (3 M KCl) reference electrode by an electrochemical analyzer (Autolab, model PGSTAT30, Eco Chemie, Utrecht, The Netherlands). All electrochemical measurements were conducted in 0.1 M phosphate buffered saline (PBS, pH = 7.0) as the supporting electrolyte in the absence and presence of acetaminophen at ambient temperature.

3. Results

The morphologies of Ni–Co–Te nanocomposites were characterized by FESEM and FETEM. FESEM imaging (Figure 1a) revealed that Ni–Co–Te nanocomposites with a mace-like structure were successfully synthesized via hydrothermal method. It confirmed that the Ni–Co–Te nanocomposites were constructed of a multi-dimensional hierarchical structure consisting of fibers (several micrometers in average length and 100~200 nm in diameter) and the surface was covered by a densely-packed short needle-like structure; this was consistent with the FETEM observation (Figure 1b,c). Owing to these unique structural features, the Ni–Co–Te nanocomposites, through the formation of rough surfaces, were endowed with a large specific surface area, which could easily be extended to expose more electrochemically active interface.

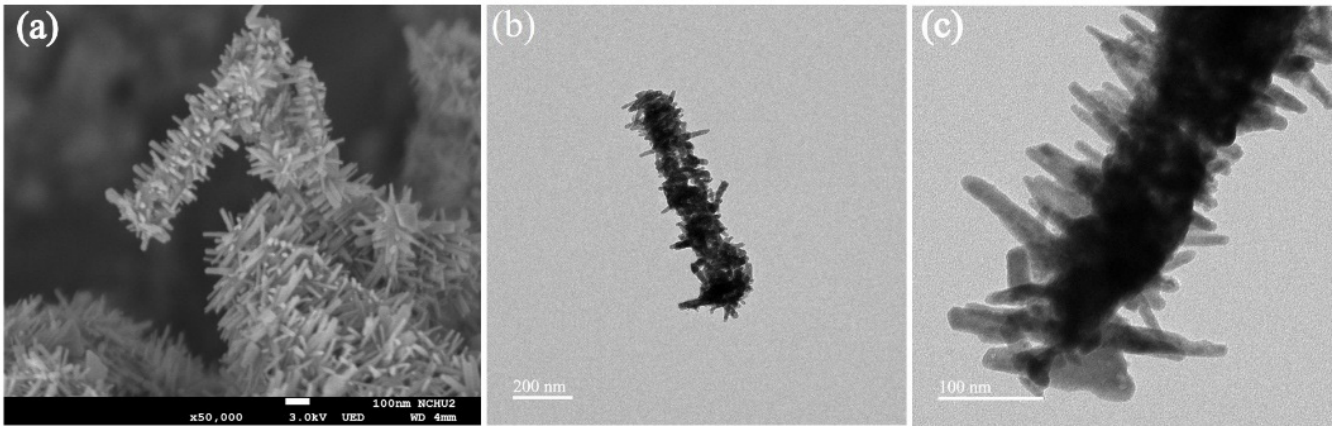

Figure 1. (**a**) FESEM, and (**b**,**c**) FETEM, images of Ni–Co–Te nanocomposites.

The structure and phase composition of Ni–Co–Te nanocomposites were characterized by XRD pattern and compared with the standard patterns of $CoNiTe_2$ (JCPDS No. 65-8961) [32], as shown in Figure 2. The XRD pattern showed five distinct diffraction peaks located at 2θ about 31.1°, 42.8°, 46.0°, 56.5°, and 58.2°, which conformed to the (101), (102), (110), (201) and (103) lattice planes of $CoNiTe_2$. The surface elemental composition and valance states of Ni–Co–Te nanocomposites were characterized by XPS, as shown in Figure 3. The full scan XPS survey spectrum of the Ni–Co–Te nanocomposites (Figure 3a) confirmed the existence of Ni 2p, Co 2p, and Te 3d elements in the Ni–Co–Te nanocomposites. In order to further characterize the chemical states of these elements, the nanocomposite was characterized in detail by high-resolution XPS spectra. The high-resolution XPS spectra of Ni 2p, Co 2p, and Te 3d of the Ni–Co–Te nanocomposites are shown in Figure 3b–d, respectively. The Ni 2p XPS spectrum (Figure 3b) was divided into two spin–orbit doublets (873.2 eV for Ni $2p_{1/2}$ and 855.4 eV for Ni $2p_{3/2}$) with a spin–orbit splitting value of 17.8. To identify the specific Ni species, the Ni $2p_{1/2}$ (Ni $2p_{3/2}$) doublets were further deconvoluted into three peaks located at 872.2 eV (852.8 eV), 873.5 eV (855.6 eV), and 879.4 eV (861.2 eV), attributed to the Ni^{2+} and Ni^{3+}, and shake-up satellite (Sat.). This implied the coexistence of Ni^{2+} and Ni^{3+} states in the Ni–Co–Te nanocomposites [33]. Figure 3c shows that the Co 2p XPS spectrum included two spin–orbit-split doublets located at 796.3 eV in Co $2p_{1/2}$ (780.6 eV in Co $2p_{3/2}$) with a spin–orbit splitting value of 15.7 eV, accompanied by two shake-up satellites (Sat.) at 802.5 eV and 786.7 eV. The Co $2p_{1/2}$ and Co $2p_{3/2}$ peaks could be further deconvoluted into two overlapping peaks corresponding to Co^{2+} and Co^{3+} located at 797.8 eV (782.6 eV) and 796.2 eV (780.5 eV), revealing that Co^{2+} and Co^{3+} oxidation states coexisted in the Ni–Co–Te nanocomposites [34]. The Te 3d XPS spectrum in Figure 3d exhibited two spin–orbit peaks of Te $3d_{3/2}$ and Te $3d_{5/2}$ at 583.2 eV and 572.8 eV, and the spectra were accompanied by two strong shake-up satellites (Sat.) located at 586.4 eV and 576.0 eV. The obvious characteristic peaks of shake-up satellites implied Te^{4+} in the Ni–Co–Te nanocomposites [35]. Therefore, the results of the above analyses demonstrate that Ni–Co–Te nanocomposites were successfully prepared and presented the best morphological and structural characteristics, which boosts their further promotion in practical applications for electrochemical sensing.

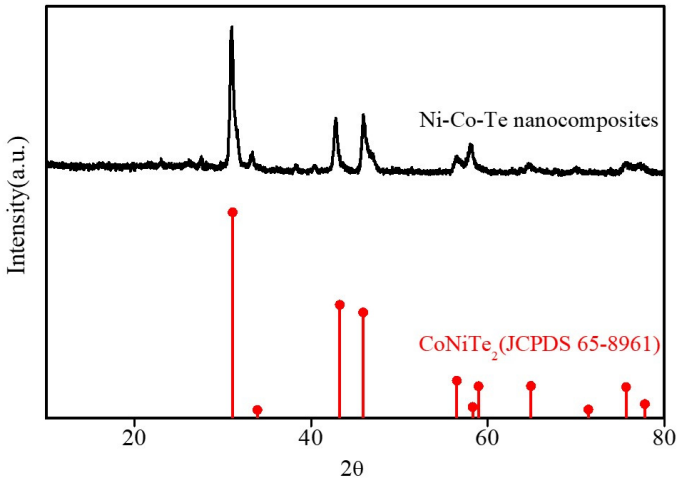

Figure 2. XRD patterns of Ni–Co–Te nanocomposites.

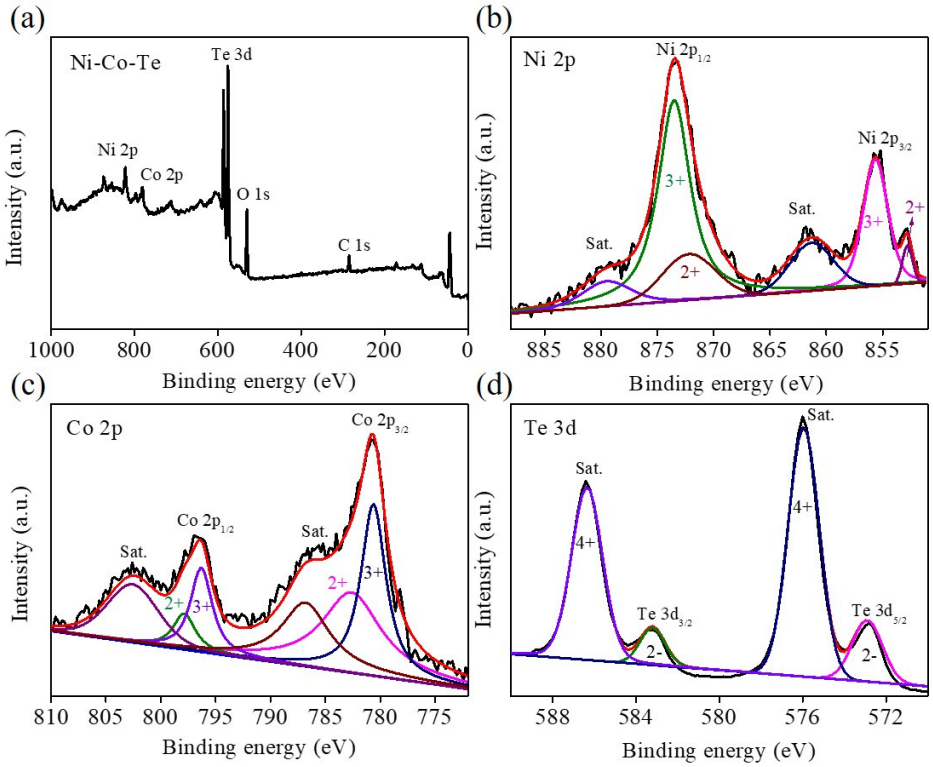

Figure 3. XPS paterns of Ni–Co–Te nanocomposites: (**a**) full scan, (**b**) Ni 2p, (**c**) Co 2p, and (**d**) Te 3d.

The electrochemical characteristics of Ni–Co–Te nanocomposites were performed by cyclic voltammetry (CV). Figure 4 shows the CV curves of bare GCE, Nafion-modified GCE, and Ni–Co–Te/Nafion-modified GCE in 0.1 M PBS (pH = 7.0) in the absence (dashed lines) and presence (solid lines) of 1 mM acetaminophen at a scan rate of 50 mV s^{-1}. In the absence of acetaminophen, no noteworthy redox peak was detected in the CV curves of these electrodes. In contrast, after adding 1 mM acetaminophen into the electrolyte, a pair of non-reversible redox peak appeared in the CV curves (expressed by the larger peak-to-peak separation and the larger difference of the anodic and cathodic peak current), indicating the non-reversible two-proton and two-electron transfer reaction mechanism of the acetaminophen/N-acetyl-p-quinoneimine redox couple (acetaminophen ↔ N-acetyl-p-quinoneimine + $2e^-$ + $2H^+$) [36]. By comparing the CV curves, Ni–Co–Te/Nafion-modified GCE exhibited obviously improved peak current and a relatively reduced peak-to-peak potential separation of redox pair, compared with bare

GCE and Nafion-modified GCE, indicating remarkable electrocatalytic activity towards the redox reaction of acetaminophen. Furthermore, as mentioned in the CV curves (Figure 4), it was also noted that Nafion-modified GCE exhibited a relatively higher electrocatalytic activity than bare GCE. Pre-concentration of the target analyte in the Nafion-modified GCE was the main reason for its good electrocatalytic performance. Nafion, as a cation exchange polymer, is deprotonated (pH > pKa = −6), and acetaminophen is protonated (pH < pKa = 9.7) in pH 7.0 PBS (in this case). Hence, it provided evidence that the electrically negatively-charged Nafion, serving as a cation exchanger, could promote the pre-concentration of acetaminophen on the surface of Nafion-modified GCE, which further improved the performance in the detection of acetaminophen [37]. Details for the anodic/cathodic peak potentials (E_{pa} and E_{pc}) and peak-to-peak separation values (ΔE_p) of the three electrodes in the presence of 1 mM acetaminophen are included in Table 1. Cyclic voltammetric study of the electrochemical redox reaction can provide a qualitative account of the degree of reversibility by comparison of the peak-to-peak separation values (ΔE_p) of the electrodes. The smallest ΔE_p values (0.34 V) of Ni–Co–Te/Nafion-modified GCE demonstrated that Ni–Co–Te nanocomposites possess relatively good reversibility. The anodic peak current observed with Ni–Co–Te/Nafion-modified GCE was approximately 27.17 μA, that is, 3.03 and 1.74 times higher than bare GCE (8.96 μA) and Nafion-modified GCE (15.59 μA). The excellent electrochemical performance of the Ni–Co–Te nanocomposites could be explained by two reasons: First, the lower electronegativity of the telluride atom in the Ni–Co–Te nanocomposites created a high degree of covalency in the metal–telluride bond. It meant that relatively lower energy was required for preceding electrochemical reactions and significantly accelerating the redox electrochemical kinetics. Second, the unique structural features of Ni–Co–Te nanocomposites also played another indispensable role in delivering a large specific surface area to expose more electrochemically active interface, thus, endowing excellent electrochemical sensing performance.

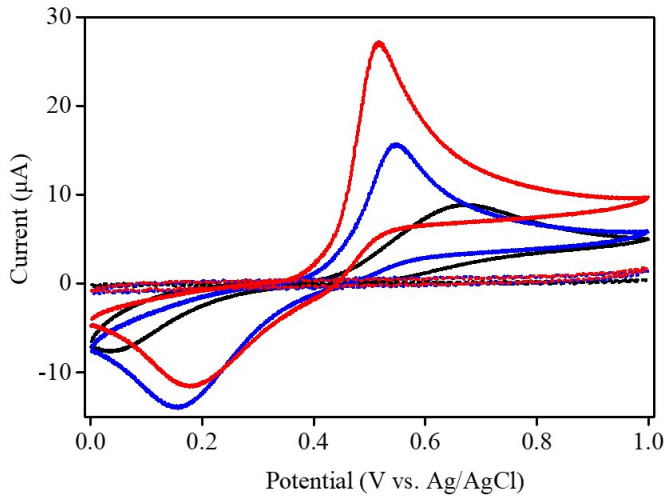

Figure 4. CV curves of bare GCE (black line), Nafion-modified GCE (blue line), and Ni–Co–Te/Nafion-modified GCE (red line) in 0.1 M PBS (pH = 7.0) in the absence (dashed lines) and presence (solid lines) of 1 mM acetaminophen at a scan rate of 50 mV s^{-1}.

Table 1. The anodic/cathodic peak potentials (E_{pa} and E_{pc}) and peak-to-peak separation values (ΔE_p) of the electrodes in the presence of 1 mM acetaminophen.

Electrodes	E_{pa} (V)	E_{pc} (V)	ΔE_p (V)
Bare GCE	0.68	0.04	0.64
Nafion-modified GCE	0.55	0.16	0.39
Ni–Co–Te/Nafion-modified GCE	0.52	0.18	0.34

In order to achieve optimal electrochemical sensing performance for the redox reaction of acetaminophen, the amounts of Ni–Co–Te nanocomposites and pH were investigated to gain better insight into the optimization of the operating parameters affecting electrochemical sensing performance. Ni–Co–Te/Nafion-modified GCE, with different amounts of Ni–Co–Te nanocomposites and pH, were characterized by CV in 0.1 M PBS (pH = 7.0) in the presence of 1 mM acetaminophen at a scan rate of 50 mV s^{-1}. The impact of the loading amount of nanocomposite was performed by adding different loading amounts of Ni–Co–Te nanocomposites (from 0.5 to 4.0 mg) into 0.5 wt % Nafion solution to form a homogenous dispersion, which was then drop cast onto the bare GCE. Figure 5a shows that the anodic peak current gradually increased with an increasing loading amount of Ni–Co–Te nanocomposites. When the loading amount of Ni–Co–Te nanocomposites exceeded 2 mg, a slight decrease in the anodic peak current was observed (see inset of Figure 5a). This decrease in peak current was due to the mass-transfer limitation of excess catalyst loading [38]. Therefore, 2 mg was selected as the best loading amount of Ni–Co–Te nanocomposites for electrochemical acetaminophen sensing. To interpret the impact of pH on electrocatalytic activity with the redox reaction of acetaminophen, CV was conducted by adjusting pH values of 0.1 M PBS (in the range of 5~9) in the presence of 1 mM acetaminophen at a scan rate of 50 mV s^{-1}. In Figure 5b, it can clearly be observed that both anodic and cathodic potentials shifted negatively with increasing pH, illustrating that the electrochemical reactions of acetaminophen involve proton transfer. A linear relationship between anodic peak potential (E_{pa}) and the pH values of PBS was also observed. The linear regression equation can be expressed as E_{pa} (V) = 0.910 − 0.053 pH (R^2 = 0.984) (see inset of Figure 5b). The slope of −0.053 pH/V is very close to the theoretical value of −0.059 pH/V, revealing that the proposed reaction mechanism of acetaminophen involved two electron/proton transfer steps, as governed by the Nernst equation [39,40]. Furthermore, the anodic peak current started to increase from pH 4.0 to 7.0 and then the anodic peak current conversely decreased (see inset of Figure 5b). Therefore, a pH value of 7.0 was considered optimum to ensure excellent catalytic activity in enhancing electrochemical acetaminophen sensing.

Figure 6 displays the CV curves of Ni–Co–Te/Nafion-modified GCE in 0.1 M PBS (pH = 7.0) in the presence of 1 mM acetaminophen at different scan rates from 50 to 300 mV s^{-1}. It can be seen that the peak current increases with the increasing scan rate, in which both anodic and cathodic peak current (I_{pa} and I_{pc}) vary linearly with the square root of the scan rate ($\upsilon^{1/2}$) (Figure 6b). Both linear regression equations can be expressed as I_{pa} (μA) = 15.333 + 1.621$\upsilon^{1/2}$ ((mV s^{-1})$^{1/2}$) (R^2 = 0.999) and I_{pc} (μA) = 1.605 − 1.608$\upsilon^{1/2}$((mV s^{-1})$^{1/2}$) (R^2 = 0.999), respectively, indicating a diffusion-controlled process of electrochemical acetaminophen reaction on Ni–Co–Te/Nafion-modified GCE [41].

Under the optimized experimental conditions, the electrochemical performance of the Ni–Co–Te/Nafion-modified GCE for acetaminophen was measured by differential pulse voltammetry (DPV) in 0.1 M PBS (pH = 7.0) with the successive addition of various acetaminophen concentrations (0~1000 μM) to estimate the applicability of the fabricated electrochemical sensing. The optimal parameters for DPV-based experiments were: potential window = 0.2~0.8 V; scan rate = 20 mVs^{-1}; modulation time = 0.05 s; interval time = 0.2 s; and step potential = 0.004 V. Figure 7a shows that Ni–Co–Te/Nafion-modified GCE exhibited a better differential pulse voltammetric response towards acetaminophen sensing. Differential pulse voltammetric response increased with respect to acetaminophen concentration up to 1000 μM. The differential pulse voltammetric response in the concentration range between 0 and 1000 μM collected to plot the corresponding calibration plot is illustrated in Figure 7b. The linear regression equation between anodic peak current (I_{pa}) and the concentration values of acetaminophen (Conc.) can be expressed as I_{pa} (μA) = 0.386 + 0.035 Conc. (μM). The calibration plot was linear from 2.5 to 1000 μM (R^2 = 0.996). The sensitivity, limit of detection (LOD) based on 3 S_b/m, and limit of quantification (LOQ) based on 10 S_b/m (S_b is the standard deviation of the blank signals for n = 3, and m is the slope of the calibration plot) can be calculated from the calibration plot and

were estimated to be 0.50 μAμM^{-1}cm^{-2}, 0.92 μM, and 3.07 μM, respectively, which were comparable to other previously reported values using transition metal compounds based materials [42–45] (Table 2).

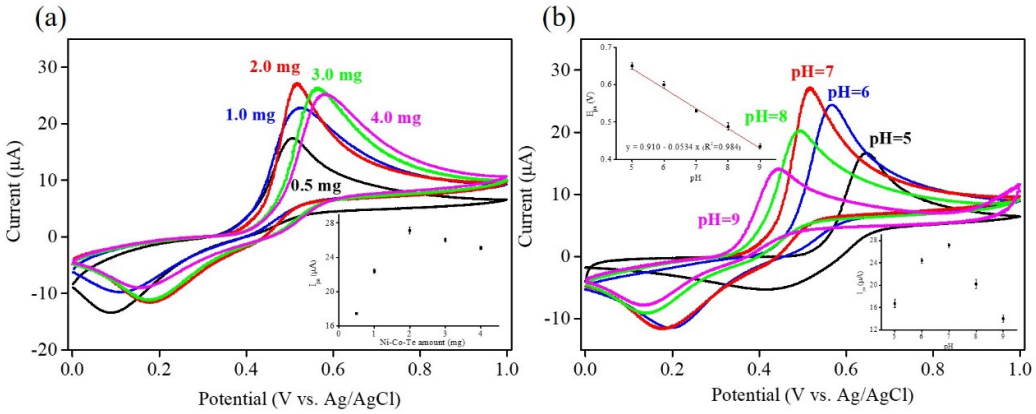

Figure 5. CV curves of Ni–Co–Te/Nafion-modified GCE with: (**a**) different amounts of Ni–Co–Te nanocomposites, and (**b**) pH in 0.1 M PBS in the presence of 1 mM acetaminophen at a scan rate of 50 mV s^{-1}. Inset of Figure 5 (**a**): plot of different amounts of Ni–Co–Te nanocomposites vs. the anodic peak current (I_{pa}). Insets of Figure 5 (**b**): plot of pH vs. the anodic peak potential (E_{pa}) (upper left inset) and plot of pH vs. the anodic peak current (I_{pa}) (bottom right inset).

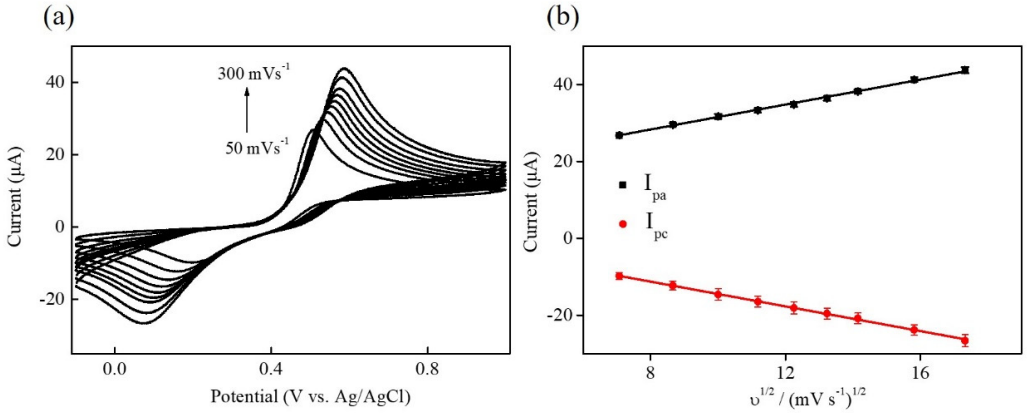

Figure 6. (**a**) CV curves of Ni–Co–Te/Nafion-modified GCE in 0.1 M PBS (pH = 7.0) in the presence of 1 mM acetaminophen at different scan rates from 50 (line a) to 300 (line i) mV s^{-1}. (**b**) The plot of the square root of the scan rate ($\upsilon^{1/2}$) vs. the anodic and cathodic peak current (I_{pa} and I_{pc}).

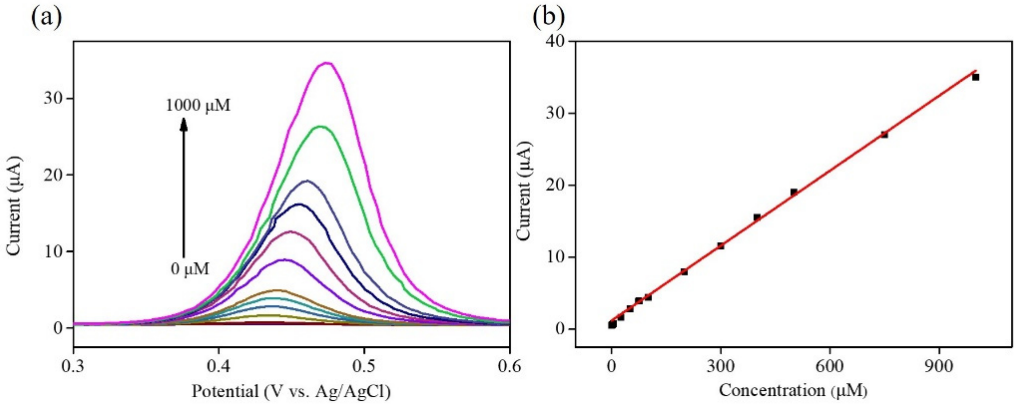

Figure 7. (**a**) DPV curves of Ni–Co–Te/Nafion-modified GCE for acetaminophen in 0.1 M PBS (pH = 7.0) with the successive addition of various acetaminophen concentrations (0~1000 μM). (**b**) Plot of acetaminophen concentration vs. the anodic peak current.

Table 2. Comparison of the performance of electrochemical acetaminophen sensing using transition metal compounds based materials.

Electrode Materials	Linear Range (μM)	Sensitivity ($\mu A \mu M^{-1} cm^{-2}$)	Limit of Detection (μM)	References
Co–Ni/Copper foam	10–100	7.96	2.70	[42]
$CuCo_2O_4$	5–5000	0.32	2.75	[43]
NiO–CuO/graphene	4–100 100–400	0.62 0.38	1.33	[44]
NiO	7.5–3000	0.09	0.23	[45]
Ni–Co–Te	2.5–1000	0.50	0.92	This work

Interfering molecules represent a challenging and significant problem related to selectivity issues in a wide variety of electrochemical sensing mechanisms. Interference from the oxidation of common interfering species present in samples (including dopamine hydrochloride (DA), uric acid (UA), D-(+)-Glucose (Glu), and L-ascorbic acid (AA), etc.) will interfere with detection and quantitative analysis of the substance. Hence, interference testing is conducted to reflect the sensing ability to discriminate the interfering species for determining the target molecule. In this study, interference testing was performed to evaluate the selectivity of Ni–Co–Te nanocomposites by differential pulse voltammetry (DPV) in 0.1 M PBS (pH = 7.0) with the presence of 5 μM DA, 5 μM UA, 5 μM Glu, 5 μM AA, and 5 μM acetaminophen (AC), respectively. As observed (Figure 8a), Ni–Co–Te/Nafion-modified GCE had the ability to discriminate the interfering species through well-separated oxidation peaks between these interfering species. It can be expected that Ni–Co–Te nanocomposites have excellent selectivity for determining the target molecule in the presence of the other interfering species. To further prove the feasibility of Ni–Co–Te nanocomposites with the interference of coexisting substances in the determination of acetaminophen, Figure 8b displays the differential pulse voltammetric response in 0.1 M PBS (pH = 7.0) with successive addition of various acetaminophen concentrations (from 5 μM to 30 μM) coexisting with 5 μM DA, 5 μM UA, 5 μM Glu, and 5 μM AA. The differential pulse voltammetric response of acetaminophen increased with respect to acetaminophen concentrations up to 30 μM, suggesting no significant effects on interfering species. It showed that Ni–Co–Te/Nafion-modified GCE exhibited a high selectivity for determining acetaminophen with negligible interfering species. The excellent selectivity was attributed to the unique structural and chemical features of Ni–Co–Te nanocomposites, which expose more electrochemically active sites to facilitate its electrocatalytic performance.

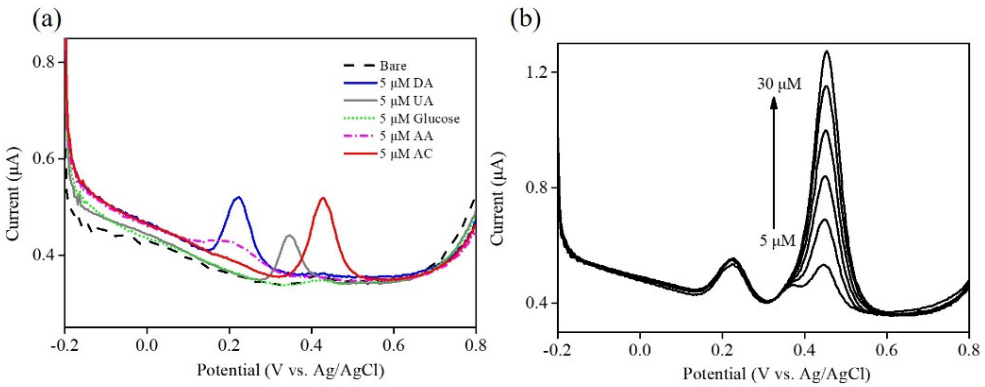

Figure 8. (**a**) Interference tests of Ni–Co–Te/Nafion-modified GCE using DPV in 0.1 M PBS (pH = 7.0) with the presence of 5 μM DA, 5 μM UA, 5 μM Glu, 5 μM AA, and 5 μM acetaminophen (AC), respectively. (**b**) Interference tests of Ni–Co–Te/Nafion-modified GCE using DPV in 0.1 M PBS (pH = 7.0) with the successive addition of various acetaminophen concentrations (from 5 μM to 30 μM) coexisting with 5 μM DA, 5 μM UA, 5 μM Glu, and 5 μM AA.

For real sample analysis, the Ni–Co–Te/Nafion-modified GCE was applied to the determination of acetaminophen concentration in commercial Panadol tablets obtained from the market (label claim: Acetaminophen 500 mg/tablet). Figure 9 displays the differential pulse voltammetric response in 0.1 M PBS (pH = 7.0) with the addition of various acetaminophen concentrations (50, 100, and 200 μM) from real samples (Panadol tablets). The preparation procedure of the tablet sample solution was as follows: each tablet containing 500 mg paracetamol was weighed and finely powdered in a mortar. The adequate amount of ground powder was transferred into a 10 mL volumetric flask and dissolved in 0.1 M PBS (pH = 7.0) to obtain final acetaminophen concentrations of 50, 100, and 200 μM. The results for real sample analyses are given in Table 3, which shows that good recovery (98.46~99.85%), precision (calculated by the relative standard deviation, RSD) (0.79~1.86%), and accuracy (calculated by relative error, RE) (0.25~1.54%) were obtained through measurements repeated three times. Therefore, Ni–Co–Te nanocomposites have accurate and reliable detection results for electrochemical acetaminophen sensing of a commercial acetaminophen tablet, illustrating that Ni–Co–Te nanocomposites have potential usefulness for practical application.

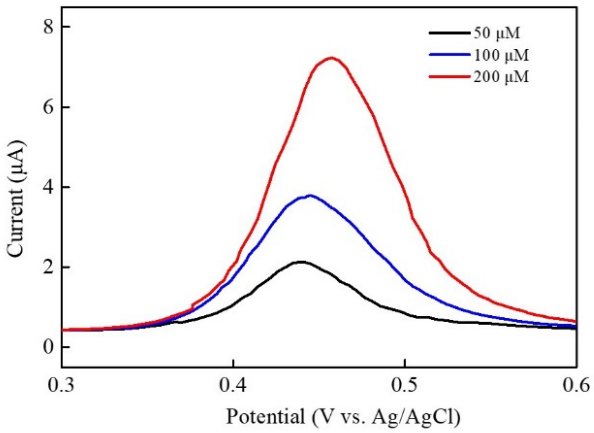

Figure 9. Real sample analysis (commercial Panadol (500 mg/tablet)) of Ni–Co–Te/Nafion-modified GCE using DPV in 0.1 M PBS (pH = 7.0) with the addition of various acetaminophen concentrations (50, 100, and 200 μM).

Table 3. Real sample analysis of Ni–Co–Te nanocomposites.

Real Sample	Added (μM)	Found by Electrochemical Sensing (μM)	Recovery [1] (%)	Precision [2] (%)	Accuracy [3] (%)
Panadol	50	49.23	98.46	1.18	1.54
	100	99.85	99.85	1.86	0.25
	200	199.33	99.67	0.79	0.34

[1] Recovery%: [Found/Added] × 100%. [2] Precision%: [Standard Deviation/Mean] × 100%. [3] Accuracy%: [(Found-Added)/Added] × 100%.

4. Conclusions

In this study, Ni–Co–Te nanocomposites were successfully prepared using a hydrothermal method. This method was also employed to prepare the best morphological and structural characteristics of Ni–Co–Te nanocomposites. The lower electronegativity of the telluride atom in Ni–Co–Te nanocomposites creates a high degree of covalency in the metal–telluride bond to significantly accelerate the redox electrochemical kinetics. The unique structural features of Ni–Co–Te nanocomposites deliver a large specific surface area to expose more electrochemically active interface, resulting in significantly improved electrochemical sensing performance (including linear range from 2.5 to 1000 μM, sensitivity

of 0.5 $\mu A \mu M^{-1} cm^{-2}$, limit of detection of 0.92 μM, and excellent selectivity). The remarkable performance of Ni–Co–Te nanocomposites provides opportunities in electrochemical acetaminophen sensing and reliability in practical electrochemical sensing application.

Author Contributions: Conceptualization, Y.-C.T.; methodology, H.-W.C. and Y.-C.T.; software, J.-J.Y. and Z.-Y.W.; validation, Y.-C.T.; formal analysis, J.-J.Y. and Z.-Y.W.; investigation, H.-W.C., J.-J.Y. and Z.-Y.W.; resources, H.-W.C. and Y.-C.T.; data curation, H.-W.C., J.-J.Y. and Z.-Y.W.; writing—original draft preparation, H.-W.C. and Y.-C.T.; writing—review and editing, H.-W.C. and Y.-C.T.; visualization, H.-W.C. and Y.-C.T.; supervision, H.-W.C. and Y.-C.T.; project administration, Y.-C.T. All authors have read and agreed to the published version of the manuscript.

Funding: Not applicable.

Institutional Review Board Statement: Not applicable.

Informed Consent Statement: Not applicable.

Data Availability Statement: Not applicable.

Acknowledgments: This study acknowledges financial support from the Ministry of Science and Technology, and National United University, Taiwan (MOST 110-2221-E-239-001-, MOST 110-2622-E-005-013, MOST 110-2221-E-005-009), and MOST 111-2221-E-005-003-.

Conflicts of Interest: The authors declare no conflict of interest.

References

1. Ghanem, C.I.; Pérez, M.J.; Manautou, J.E.; Mottino, A.D. Acetaminophen from liver to brain: New insights into drug pharmacological action and toxicity. *Pharmacol. Res.* **2016**, *109*, 119–131. [CrossRef] [PubMed]
2. Offor, S.J.; Amadi, C.N.; Chijioke-Nwauche, I.; Manautou, J.E.; Orisakwe, O.E. Potential Deleterious Effects of Paracetamol Dose Regime Used in Nigeria Versus That of the United States of America. *Toxicol. Rep.* **2022**, *9*, 1035–1044. [CrossRef]
3. Henderson, A.J.; Shaheen, S.O. Acetaminophen and asthma. *Paediatr. Respire. Rev.* **2013**, *14*, 9–16. [CrossRef] [PubMed]
4. Thiele, K.; Solano, M.E.; Huber, S.; Flavell, R.A.; Kessler, T.; Barikbin, R.; Jung, R.; Karimi, K.; Tiegs, G.; Arck, P.C. Prenatal acetaminophen affects maternal immune and endocrine adaptation to pregnancy, induces placental damage, and impairs fetal development in mice. *Am. J. Pathol.* **2015**, *185*, 2805–2818. [CrossRef]
5. Badar, Z.; Shanableh, A.; El-Keblawy, A.; Mosa, K.A.; Semerjian, L.; Mutery, A.A.; Hussain, M.I.; Bhattacharjee, S.; Tsombou, F.M.; Ayyaril, S.S. Assessment of Uptake, Accumulation and Degradation of Paracetamol in Spinach (*Spinacia oleracea* L.) under Controlled Laboratory Conditions. *Plants* **2022**, *11*, 1626. [CrossRef]
6. Tran, H.N.; Tomul, F.; Ha, N.T.H.; Nguyen, D.T.; Lima, E.C.; Le, G.T.; Chang, C.-T.; Masindi, V.; Woo, S.H. Innovative spherical biochar for pharmaceutical removal from water: Insight into adsorption mechanism. *J. Hazard. Mater.* **2020**, *394*, 122255. [CrossRef]
7. Stucchi, M.; Rigamonti, M.G.; Carnevali, D.; Boffito, D.C. A Kinetic Study on the Degradation of Acetaminophen and Amoxicillin in Water by Ultrasound. *Chem. Sel.* **2020**, *5*, 14986–14992. [CrossRef]
8. Kucera, K.; Jessop, A.; Alvarez, N.; Gortler, D.; Light, D. Rapid and fast-release acetaminophen gelcaps dissolve slower than acetaminophen tablets. *Adv. Inv. Pha. Medic.* **2018**, *1*, 63–71.
9. Shen, X.; Chen, X.; Wang, J.; Sun, X.; Dong, S.; Li, Y.; Yan, Y.; Wang, J.; Yuan, Q. Design and construction of an artificial pathway for biosynthesis of acetaminophen in Escherichia coli. *Metab. Eng.* **2021**, *68*, 26–33. [CrossRef]
10. Cook, S.F.; King, A.D.; van den Anker, J.N.; Wilkins, D.G. Simultaneous quantification of acetaminophen and five acetaminophen metabolites in human plasma and urine by high-performance liquid chromatography–electrospray ionization–tandem mass spectrometry: Method validation and application to a neonatal pharmacokinetic study. *J. Chromatogr. B* **2015**, *1007*, 30–42.
11. Ziemons, E.; Mantanus, J.; Lebrun, P.; Rozet, E.; Evrard, B.; Hubert, P. Acetaminophen determination in low-dose pharmaceutical syrup by NIR spectroscopy. *J. Pharm. Biomed. Anal.* **2010**, *53*, 510–516. [CrossRef]
12. Doğan, B.; Elik, A.; Altunay, N. Determination of paracetamol in synthetic urea and pharmaceutical samples by shaker-assisted deep eutectic solvent microextraction and spectrophotometry. *Microchem. J.* **2020**, *154*, 104645. [CrossRef]
13. Cao, F.; Zhang, M.; Yuan, S.; Feng, J.; Wang, Q.; Wang, W.; Hu, Z. Transformation of acetaminophen during water chlorination treatment: Kinetics and transformation products identification. *Environ. Sci. Pollut. Res.* **2016**, *23*, 12303–12311. [CrossRef]
14. Kantize, K.; Booysen, I.N.; Mambanda, A. Electrochemical sensing of acetaminophen using nanocomposites comprised of cobalt phthalocyanines and multiwalled carbon nanotubes. *J. Electroanal. Chem.* **2019**, *850*, 113391. [CrossRef]
15. Ipekci, H.H.; Ozcan, M.; Turkyilmaz, B.G.; Uzunoglu, A. Ni/NiO/Ni–B/graphene heterostructure-modified electrodes and their electrochemical activities towards acetaminophen. *Anal. Methods* **2021**, *13*, 3187–3195. [CrossRef]
16. Wei, M.; Lu, W.; Liu, G.; Jiang, Y.; Liu, X.; Bai, L.; Cao, X.; Jia, J.; Wu, H. Ni2P nanosheets: A high catalytic activity platform for electrochemical detection of acetaminophen. *Chin. J. Chem.* **2021**, *39*, 1849–1854. [CrossRef]

17. Antoniazzi, C.; de Lima, C.A.; Marangoni, R.; de Castro, E.G.; Santana, E.R.; Spinelli, A. Molybdenum trioxide incorporated in a carbon paste as a sensitive device for bisphenol A monitoring. *Microchem. J.* **2020**, *159*, 105528. [CrossRef]
18. Zamarchi, F.; Vieira, I.C. Determination of paracetamol using a sensor based on green synthesis of silver nanoparticles in plant extract. *J. Pharm. Biomed. Anal.* **2021**, *196*, 113912. [CrossRef]
19. Wang, L.; Meng, T.; Fan, Y.; Chen, C.; Guo, Z.; Wang, H.; Zhang, Y. Electrochemical study of acetaminophen oxidation by gold nanoparticles supported on a leaf-like zeolitic imidazolate framework. *J. Colloid Interface Sci.* **2018**, *524*, 1–7. [CrossRef]
20. Zhang, X.; Wang, K.-P.; Zhang, L.-N.; Zhang, Y.-C.; Shen, L. Phosphorus-doped graphene-based electrochemical sensor for sensitive detection of acetaminophen. *Anal. Chim. Acta* **2018**, *1036*, 26–32. [CrossRef]
21. Adhikari, B.-R.; Govindhan, M.; Chen, A. Sensitive detection of acetaminophen with graphene-based electrochemical sensor. *Electrochim. Acta* **2015**, *162*, 198–204. [CrossRef]
22. Wang, K.; Wu, C.; Wang, F.; Jing, N.; Jiang, G. Co/Co_3O_4 nanoparticles coupled with hollow nanoporous carbon polyhedrons for the enhanced electrochemical sensing of acetaminophen. *ACS Sustain. Chem. Eng.* **2019**, *7*, 18582–18592. [CrossRef]
23. Lu, Z.; Zhong, J.; Zhang, Y.; Sun, M.; Zou, P.; Du, H.; Wang, X.; Rao, H.; Wang, Y. MOF-derived Co_3O_4/$FeCo_2O_4$ incorporated porous biomass carbon: Simultaneous electrochemical determination of dopamine, acetaminophen and xanthine. *J. Alloys Compd.* **2021**, *858*, 157701. [CrossRef]
24. Wu, Q.; He, L.; Jiang, Z.W.; Li, Y.; Cao, Z.M.; Huang, C.Z.; Li, Y.F. CuO nanoparticles derived from metal-organic gel with excellent electrocatalytic and peroxidase-mimicking activities for glucose and cholesterol detection. *Biosens. Bioelectron.* **2019**, *145*, 111704. [CrossRef]
25. Kaur, B.; Anu Prathap, M.; Srivastava, R. Synthesis of transition-metal exchanged nanocrystalline ZSM-5 and their application in electrochemical oxidation of glucose and methanol. *ChemPlusChem* **2012**, *77*, 1119–1127. [CrossRef]
26. Dong, Q.; Yang, L.; He, Z.; Zhang, Y.; Tang, X.; Tang, J.; Huang, K.; Zou, Z.; Xiong, X. Co-Based Transition Metal Hydroxide Nanosheet Arrays on Carbon Cloth for Sensing Glucose and Formaldehyde. *ACS Appl. Nano Mater.* **2021**, *4*, 5076–5083. [CrossRef]
27. Li, Z.; Mi, H.; Ji, C.; Guo, F.; Qiu, P.; Ma, K.; He, S.; Wu, D.; Cui, H.; Yang, N. Phosphate-modified Co–Ni phosphide heterostructure formed by interfacial and electronic tuning for boosted faradaic properties. *Dalton Trans.* **2021**, *50*, 5036–5043. [CrossRef]
28. Kim, M.; Ju, H.; Kim, J. Highly efficient bifunctional catalytic activity of bismuth rhodium oxide pyrochlore through tuning the covalent character for rechargeable aqueous Na–air batteries. *J. Mater. Chem. A* **2018**, *6*, 8523–8530. [CrossRef]
29. Amorim, I.; Liu, L. Transition metal tellurides as emerging catalysts for electrochemical water splitting. *Curr. Opin. Electrochem.* **2022**, *34*, 101031. [CrossRef]
30. Brea, C.; Hu, G. Shifting and breaking scaling relations at transition metal telluride edges for selective electrochemical CO_2 reduction. *J. Mater. Chem. A* **2022**, *10*, 10162–10170. [CrossRef]
31. Park, G.D.; Kang, Y.C. Conversion reaction mechanism for yolk-shell-structured iron telluride-C nanospheres and exploration of their electrochemical performance as an anode material for potassium-ion batteries. *Small Methods* **2020**, *4*, 2000556. [CrossRef]
32. Qian, G.; Mo, Y.; Yu, C.; Zhang, H.; Yu, T.; Luo, L.; Yin, S. Free-standing bimetallic CoNiTe2 nanosheets as efficient catalysts with high stability at large current density for oxygen evolution reaction. *Renew. Energy* **2020**, *162*, 2190–2196. [CrossRef]
33. Han, Y.; Zhou, J.; Wang, L.; Xing, L.; Xue, Z.; Jiao, Y.; Pang, Y. Redox-active nanostructure electrode of Mn/Ni bimetal organic frameworks anchoring on multi-walled carbon nanotubes for advanced supercapacitor. *J. Electroanal. Chem.* **2021**, *882*, 114993. [CrossRef]
34. Patil, S.A.; Hussain, S.; Shrestha, N.K.; Mengal, N.; Jalalah, M.; Jung, J.; Park, J.-G.; Choi, H.; Kim, H.-S.; Noh, Y.-Y. Facile synthesis of cobalt–nickel sulfide thin film as a promising counter electrode for triiodide reduction in dye-sensitized solar cells. *Energy* **2020**, *202*, 117730. [CrossRef]
35. Lin, C.-Y.; Ulaganathan, R.K.; Sankar, R.; Murugesan, R.C.; Subramanian, A.; Rozhin, A.; Firdoz, S. Silicon-based two-dimensional chalcogenide of p-type semiconducting silicon telluride nanosheets for ultrahigh sensitive photodetector applications. *J. Mater. Chem. C* **2021**, *9*, 10478–10486. [CrossRef]
36. Zheng, M.; Gao, F.; Wang, Q.; Cai, X.; Jiang, S.; Huang, L.; Gao, F. Electrocatalytical oxidation and sensitive determination of acetaminophen on glassy carbon electrode modified with graphene–chitosan composite. *Mater. Sci. Eng. C* **2013**, *33*, 1514–1520. [CrossRef]
37. Martínez-Huitle, C.; Fernandes, N.S.; Ferro, S.; De Battisti, A.; Quiroz, M. Fabrication and application of Nafion®-modified boron-doped diamond electrode as sensor for detecting caffeine. *Diamond Relat. Mater.* **2010**, *19*, 1188–1193. [CrossRef]
38. Deng, Z.-P.; Sun, Y.; Wang, Y.-C.; Gao, J.-D. A NiFe alloy reduced on graphene oxide for electrochemical nonenzymatic glucose sensing. *Sensors* **2018**, *18*, 3972. [CrossRef]
39. Fan, Y.; Liu, J.-H.; Yang, C.-P.; Yu, M.; Liu, P. Graphene–polyaniline composite film modified electrode for voltammetric determination of 4-aminophenol. *Sens. Actuators B Chem.* **2011**, *157*, 669–674. [CrossRef]
40. Fu, L.; Lai, G.; Yu, A. Preparation of β-cyclodextrin functionalized reduced graphene oxide: Application for electrochemical determination of paracetamol. *Rsc Adv.* **2015**, *5*, 76973–76978. [CrossRef]
41. Huang, T.-Y.; Kung, C.-W.; Wei, H.-Y.; Boopathi, K.M.; Chu, C.-W.; Ho, K.-C. A high performance electrochemical sensor for acetaminophen based on a rGO–PEDOT nanotube composite modified electrode. *J. Mater. Chem. A* **2014**, *2*, 7229–7237. [CrossRef]
42. Premlatha, S.; Bapu, G.R. Fabrication of Co-Ni alloy nanostructures on copper foam for highly sensitive amperometric sensing of acetaminophen. *J. Electroanal. Chem.* **2018**, *822*, 33–42. [CrossRef]

43. Samanta, S.; Srivastava, R. Simultaneous determination of epinephrene and paracetamol at copper-cobalt oxide spinel decorated nanocrystalline zeolite modified electrodes. *J. Colloid Interface Sci.* **2016**, *475*, 126–135. [CrossRef]
44. Liu, B.; Ouyang, X.; Ding, Y.; Luo, L.; Xu, D.; Ning, Y. Electrochemical preparation of nickel and copper oxides-decorated graphene composite for simultaneous determination of dopamine, acetaminophen and tryptophan. *Talanta* **2016**, *146*, 114–121. [CrossRef]
45. Annadurai, K.; Sudha, V.; Murugadoss, G.; Thangamuthu, R. Electrochemical sensor based on hydrothermally prepared nickel oxide for the determination of 4-acetaminophen in paracetamol tablets and human blood serum samples. *J. Alloys Compd.* **2021**, *852*, 156911. [CrossRef]